Bonding of Aluminum Alloys in Compound Casting

JIAN FENG, BING YE, LIJIE ZUO, QUDONG WANG, QIGUI WANG,
HAIYAN JIANG, and WENJIANG DING

The influence of the coating materials, coating thickness, and casting process on the interfacial microstructure and mechanical properties of the overcast A6061 bars with aluminum A356 and A6061 alloys was studied by OM, SEM/EDS, and mechanical testing. Results indicate that Ni coating has better thermal stability than Cu coating that heavily reacts with liquid Al alloy and forms a reaction zone around 130–150 μm during gravity casting. In the gravity casting, coarse and cracked Al$_3$Ni phase distributes along the interfacial region and degrades the mechanical properties of the overcast joints. In squeeze casting, however, fine and dispersed Ni-rich strengthening phases form uniformly in the interfacial zone and improve the metallurgical bonding of the joints. The heat transition and application of pressure during solidification are two key factors in determining the integrity and mechanical properties of the overcast joints.

I. INTRODUCTION

THE increasing demand for lightweight structures in automotive and aerospace industries has led to the wide application of aluminum (Al) alloys.[1–3] Because of the structure complexity and particularly variation in local material property requirement, one single type of Al alloy does not satisfy the component service demand.[4,5] The common solution for this problem is to form a structure by joining dissimilar metals with different fabrication procedures, such as friction stir welding (FSW),[6–8] gas metal arc welding (GMAW),[9–11] and laser beam machining (LBM).[12–15] Although those joining techniques can provide good weld quality and production flexibility with less energy input, the complex welding process and limitations in workpiece geometry and dimension have limited their wide applications.[16–18] Compound casting is a relatively simple and cost-effective processing. It achieves the bonding of two metals by casting the liquid material over the solid material, and forms a continuous metallic transition zone between two metals.[19,20]

Nevertheless, Al alloys are difficult to bond during compound casting process. Owing to the formation of oxide layer on the surface of Al alloys, the wettability of the liquid Al on the solid Al is rather poor during overcasting.[10,21] Papis et al.[22] introduced zinc layer on the Al alloy substrate to obtain the bonding of wrought and cast Al alloys. The Zn layer acts as a barrier to replace the oxide layer on the Al alloys, improving the wettability of the substrate and promoting the formation of continuous and flawless metallic interfaces. Runber et al.[23] further investigated the effect of Zn layers with various thickness on Al/Al compounds during high-pressure die casting. It was reported that the initial thickness of the Zn layer has strong influence on the microstructure and thickness of the reaction diffusion zone, but interestingly exerts little effect on mechanical properties of the compounds. Liu et al.[24] studied the effect of Zn layer thickness on the microstructure and mechanical properties of the joints under pressure by squeeze casting. The tensile strength of the joints was improved by 10 pct with squeeze casting compared to that by gravity casting.

Because of the relatively low thermal stability of the Zn layer, the casting has to be precisely controlled to get good quality joint. As a result, more research has been devoted to different coating materials that are able to sustain the liquid Al during overcasting process. Ni and Cu coating has been reported in the literature in bonding of dissimilar metals, such as Fe/Al, Ti/steel, and Mo/Cu.[25–29] Nonetheless, the application of Ni and Cu coating in bonding of lightweight alloys like aluminum is still limited. Zhang et al.[17] first introduced the Ni layer to obtain the diffusion bonding of Mg/Al couples. The diffusion distance of Ni in Al alloy is about 5 μm at 713 K (440 °C) for 90 minutes under the pressure of 1 MPa. The microhardness of the transition zone between Al and Ni is about three times higher than that of the Al matrix due to the formation of high

JIAN FENG, BING YE, LIJIE ZUO, QUDONG WANG, HAIYAN JIANG, and WENJIANG DING are with the National Engineering Research Center of Light Alloy Net Forming and State Key Laboratory of Metal Matrix Composites, Shanghai Jiao Tong University, Shanghai 200240, P.R. China. Contact e-mail: bingye@sjtu.edu.cn QIGUI WANG is with General Motors Global Propulsion Systems, 800 North Glenwood Ave, Pontiac, MI 48340-2920.

thermal stability Al₃Ni intermetallic. Wang et al.[12] employed the Ni coating to merge Mg to Al joints by the laser-arc-adhesive hybrid welding and found the enhanced mechanical properties of the joints in the presence of Ni layer. Sun et al.[30] attained the bonding of Al and Mg alloys using the Ni interlayer by resistance spot welding to impede the reaction between Al and Mg. In the interfacial zone, the continuous submicron Al₃Ni intermetallic reaction layer was detected, and Al-Al₃Ni eutectic structure dramatically increased the strength of the joints. Although many studies have been focused on the bonding of solid lightweight alloys via different methods, the application of Ni coating to enhance the bonding strength of the joints during compound casting is still of great demand.

In this work, both Ni and Cu coatings are used to improve the bonding quality between solid wrought A6061 bar and overcast liquid aluminum alloys. The influence of the coating materials, coating thickness, and casting process on the microstructure and mechanical properties of the joints is studied.

II. EXPERIMENTAL PROCEDURE

A. Materials and Surface Treatment

Wrought A6061 bars and cast Al alloys, including A356 alloy and A6061 alloy, were used to prepare the Al/Al joints during compound casting. Wrought A6061 bars were cut into rectangular bars with a dimension of $50 \times 10 \times 3$ mm³. After mechanically polished by 1000 grit sandpaper, all the samples were subjected to ultrasonic cleaning for 20 minutes and then dried in a warm air stream.

After cleaning, the A6061 bars were further degreased in the solution of 25 g/L Na₂CO₃ and 30 g/L NaHCO₃ at 338 K (65 °C) for 5 minutes before galvanization treatment. The bars were then subjected to alkali erosion, acid pickling, first-time dip galvanization, zinc retreat, and second-time dip galvanization. Subsequently, the bars were electroplated with Ni for varied times to obtain different thicknesses of Ni layer (1, 3, 5, 10, 40 μm). For comparison, the Cu layer was also introduced with a thickness of 40 μm.

B. Compound Casting Process

In this study, the wrought A6061 solid bars were overcast with both cast A356 and A6061 alloy. The cast A356 alloy was used only in gravity casting with both Ni and Cu coatings, while the A6061 alloy was used in both gravity and squeeze castings with Ni coating only.

Figure 1 is a schematic illustration of overcast Al alloys to wrought A6061 bars by gravity casting (a, b) and squeeze casting (c). In gravity casting, the A6061 bars (in green) were inserted in the slots of the rectangular steel mold 1, which was placed at the bottom of steel mold 2. The plate casting sections near A6061 bars located at both ends of mold 1 were used to perform the tensile testing. The other two areas that are located in the center of mold 1 were used for microstructure evaluation. In squeeze casting, an 80-ton vertical hydraulic press was used for direct squeeze casting. As
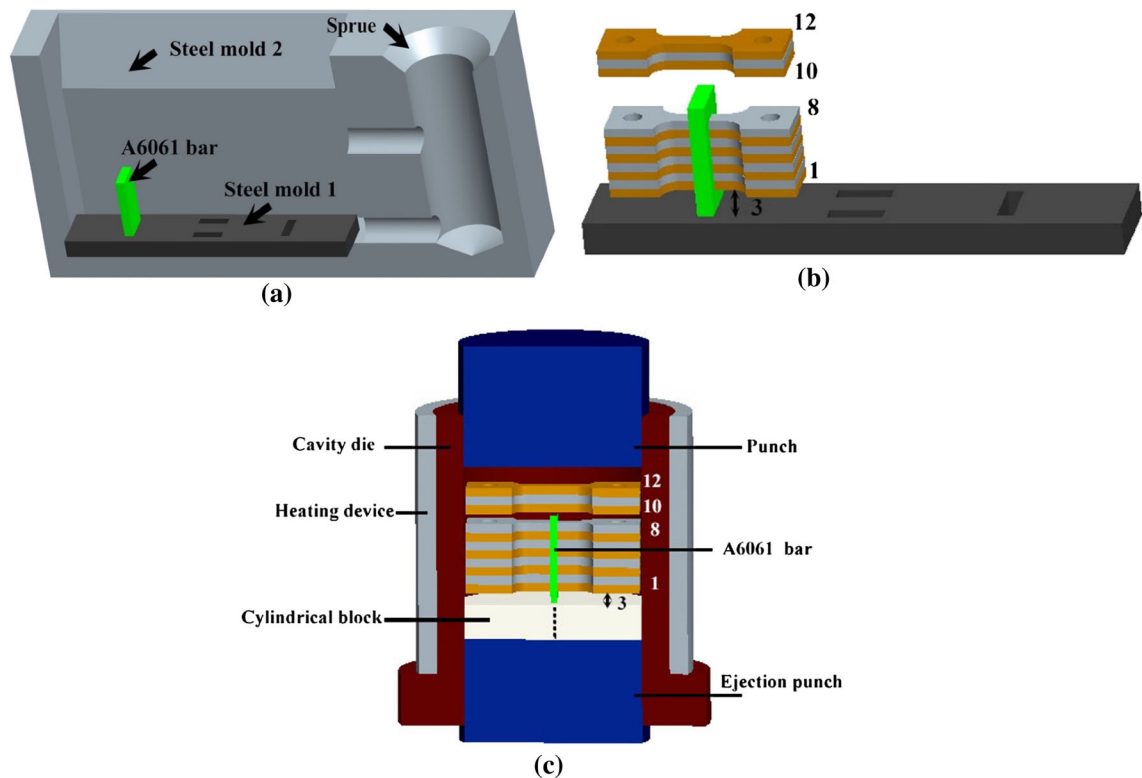

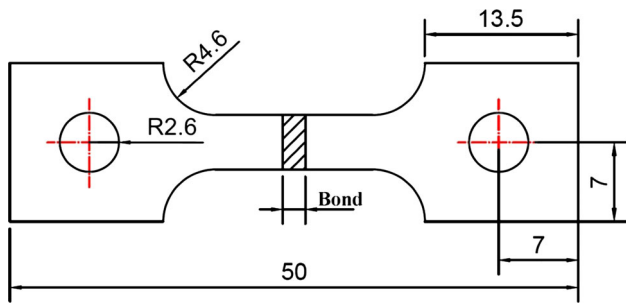Fig. 1—Schematic illustration of the gravity casting (a, b) and squeeze casting (c).

Fig. 2—The dimension of the tensile specimen in mm.

shown in Figure 1(c), the A6061 bar (in green) was pre-seated along the axial direction of a cylindrical block before pouring the liquid A6061 alloy. The cylindrical block is composed of two halves and the center of the block has a rectangle hole with a width of 3 mm and length of 10 mm. In squeeze casting, the melt was subjected to 30 MPa pressure during solidification. The pouring temperature is kept at 993 K (720 °C) for both gravity casting and squeeze casting.

Figures 1(b) and (c) display the tensile specimens extracted across the interfacial zone in both gravity cast plates and squeeze cast cylinders. Eight specimens with a typical thickness of 2.5 mm were machined from each plate or cylinder along the direction parallel to the Al bar, and designated as specimens #1 to #8 representing various distances from the bottom to the top of the Al bar. In both gravity casting and squeeze casting, the tensile specimen #1 was 3 mm offset from the mold 1 (Figure 1(a)) or the cylindrical block (Figure 1(c)) during compound casting. Tensile specimens #10 to #12 are used to test overcast base metal properties.

C. Metallurgical Analysis and Mechanical Testing

The coating surface quality and the interfacial microstructure of the overcast joints were examined using a ZEISS (Axio observer A1) optical microscope and a FEI-QUANTA250 scanning electron microscope (SEM) equipped with energy-dispersive X-ray spectroscopy (EDS). Phase identification of the fractography was performed using a RigakuUltima IV X-Ray diffractometer (Cu Kα, λ = 1.54056 Å) with the scanning range of 20 to 90 deg at a scan speed of 2 deg/min, and the XRD analyses for different Ni layer thicknesses were performed with a scan speed of 5 deg/min. The reported measurement data of coating layer thickness and the width of the reaction zone is an average value of ten measurements.

The dimensions of the tensile specimen (in mm) are shown in Figure 2, and the thickness of the tensile specimen is 2.5 mm. Tensile specimens were prepared using electrical discharge machining (EDM) to make sure the overcast Al bar to be located at the center of the gage section. The bonding strength of the overcast joints was tested on WDW-10S universal tensile tester (Jinan TE, Shandong, China) with a cross-board speed of 0.45 mm/min. Microhardness test across the interfacial zone was performed on a Zwick/Roell-HV2000 hardness tester with a load of 10 g and a dwell time of 10 seconds.

III. RESULTS

A. Coating Materials

Figure 3 shows SEM images of the overcast joints prepared by casting liquid A356 alloy over the solid A6061 bar during gravity casting. The cross-section of the overcast joint of cast aluminum A356 and A6061 bar electroplated with a 10-μm-thick Ni coating is shown in Figures 3(a) and (b). A continuous and uniform interface formed between the A6061 bar and the Ni layer. Ni diffuses into the solid Al bar by forming a diffusion reaction zone with a limited depth of 3 to 5 μm. The EDS analysis of point 1 in the diffusion zone shows a composition of 71.6 at. pct Al and 28.4 at. pct Ni, which confirms the existence of Al_3Ni intermetallic phases. The cross-section of overcast A6061 bar electroplated with a 40-μm-thick Cu coating is shown in Figures 3(c) and (d). A large diffusion zone is observed in the Al bar wherein the phase located in front of the reaction zone is Al_2Cu with a composition of 68.9 at. pct Al and 31.1 at. pct Cu. Accompanied with abundant intermetallic compounds, this diffusion zone is very wide, typically in the range of 130 to 150 μm. In some regions, the reaction diffusion zone completely disrupts the Cu layer.

Comparing the reaction diffusion zone of Ni and Cu-coated Al bar, the 10 μm Ni coating can sustain the impact of molten A356 Al alloy and forms a 3- to 5-μm transition zone which mainly consists of Al_3Ni. In the case of Cu coating, however, violent reaction happened between the A6061 bar and Cu coating even after the Cu layer thickness is increased to 40 μm. The width of the transition zone reaches 130 to 150 μm, which is much larger than that of the Ni coating. As discussed in Reference 31 the formation of wider Cu-rich reaction zone is detrimental to mechanical properties of the joints. Considering that the Ni coating offers more robustness than Cu coating, further investigation in this work will be focused on Ni coating.

Figure 4 shows the OM and SEM images of the A6061 bar, which was electroplated with 3 μm Ni layer. As shown in Figure 4(a), though the surface of A6061 substrate was mechanically polished by 320 grit sandpaper, a continuous Ni layer was successfully formed on the polished surface of Al bar. The protrusions with different dimensions demonstrate a good conformability of the Ni layer with the wrought Al substrate. The thickness of Ni layer is 3.5 ± 0.4 μm, indicating that the Ni layer thickness is well controlled by electroplating time. Figure 4(b) shows the coated surface of 3 μm Ni layer with the typical cellular interface structure. XRD results of the A6061 bars covered with different Ni layer thicknesses are shown in Figure 4(c). It is obvious that peaks of Ni increase with the varied Ni layer thickness from 1 μm to 5 μm, and the existence of Ni is confirmed. Further increasing the Ni layer to 40 μm, the peaks of Al disappear, which means that the Ni layer is thick

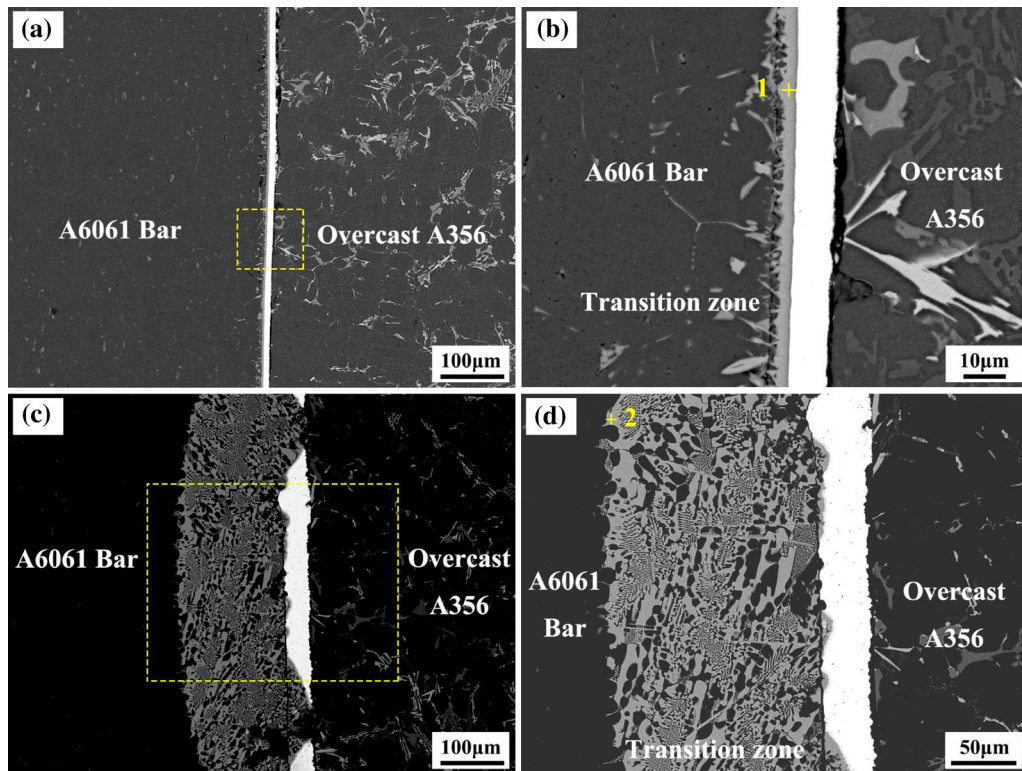Fig. 3—SEM images of the overcast joints with 10 μm Ni layer (*a*, *b*) and 40 μm Cu layer (*c*, *d*) by gravity casting.
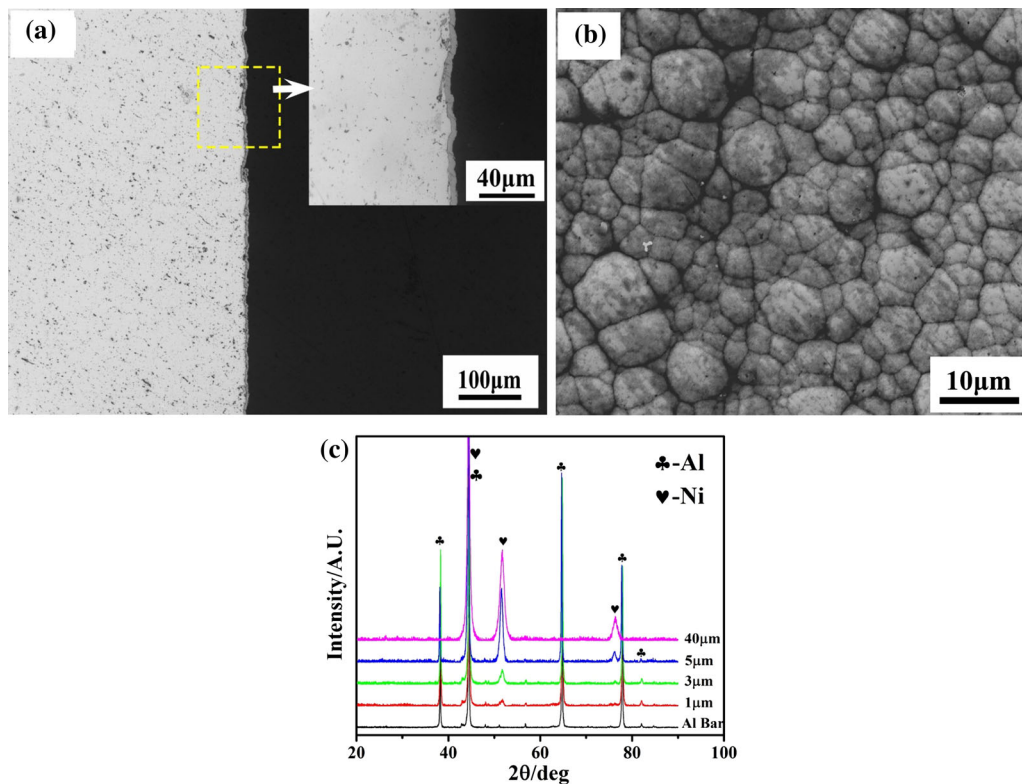

Fig. 4—The OM and SEM images of the A6061 bar with 3 μm Ni layer: (*a*) cross-section of the Ni layer, (*b*) coated surface of the Ni layer, and (*c*) XRD results for varied Ni layer thickness.

enough, and the surface of the Al bar is covered with a continuous and dense Ni layer.

B. Overcast Interfacial Microstructure

1. Effect of coating thickness

As mentioned above, the width of the diffusion reaction zone with 10-μm-thick Ni coating is limited to 3 to 5 μm, which means that a Ni layer of 3 to 5 μm thickness is enough to sustain the impact of the liquid Al alloys. For comparison purpose, a 1-μm-thick Ni layer is included in this study. In order to clearly observe the interfacial zone, the liquid Al alloy was changed from A356 to A6061 alloy although A356 is a typical casting alloy in practice.

Figure 5 shows the optical microstructure of the joints fabricated with Ni layer of 1, 3, and 5 μm, respectively. In Figure 5(a), the transition zone moves about 30 to 40 μm forward to the direction of A6061 bar with the Ni layer of 1 μm. It means that the Ni layer is too thin to sustain the thermal impact of the liquid A6061, and no obvious Ni-rich intermetallic phase forms near the interfacial zone. Along with the increased Ni layer thickness to 3 μm, discontinuous intermetallic phase forms in the interfacial zone and no obvious reaction diffusion zone is observed in Figure 5(b). However, further increasing the Ni layer thickness to 5 μm, a continuous Ni-rich interlayer forms in the interfacial region and the width reaches 5.4 $\pm$ 0.6 μm, indicating that the Ni layer is thick enough to withstand the impact of liquid A6061 and protect the A6061 bar. Furthermore, no obvious oxide inclusions and other defects were detected in the interfacial region for all overcast

joints. It is shown that the A6061 bar attains a good bond with the liquid A6061, and the oxidation of Al bar is negligible during gravity casting. Comparing Figures 5(b) and (c), discontinuous interfacial microstructure is beneficial to the mechanical properties of the joints rather than the continuous interlayer. Hence, the optimal Ni layer thickness is 3 to 5 μm.

2. Effect of fabrication process

Squeeze casting was introduced to further improve the mechanical properties of overcast joints. Figure 6 shows the optical microstructure of the joints with 3 μm Ni layer during squeeze casting. The metallographic samples were etched with Keller solution for 15 seconds to show the second phases clearly in the interfacial zone. In Figures 6(a) and (b), a large amount of intermetallic phase in black enriches in the interfacial zone and forms a reaction diffusion zone around 100 to 200 μm. Contrast to the discontinuous interfacial microstructure in Figure 5(b), most fine and dispersed intermetallic phases diffuse into the A6061 bar and enhance the mechanical properties of the joints. In Figures 6(c) and (d), Ni element also diffuses into the A6061 and increases the strength of overcast A6061 material. The microstructure observation also shows that squeeze casting produces better overcast joints of 3 μm Ni layer compared with gravity casting.

Figure 7 shows SEM micrographs of the overcast joints with 3 μm Ni layer made by both gravity casting (a, b) and squeeze casting (c, d). The EDS results of the corresponding points in Figure 7 are also listed in Table I. In gravity overcast joints, a large amount of coarse and cracked Al_3Ni phase (Point A) forms in the
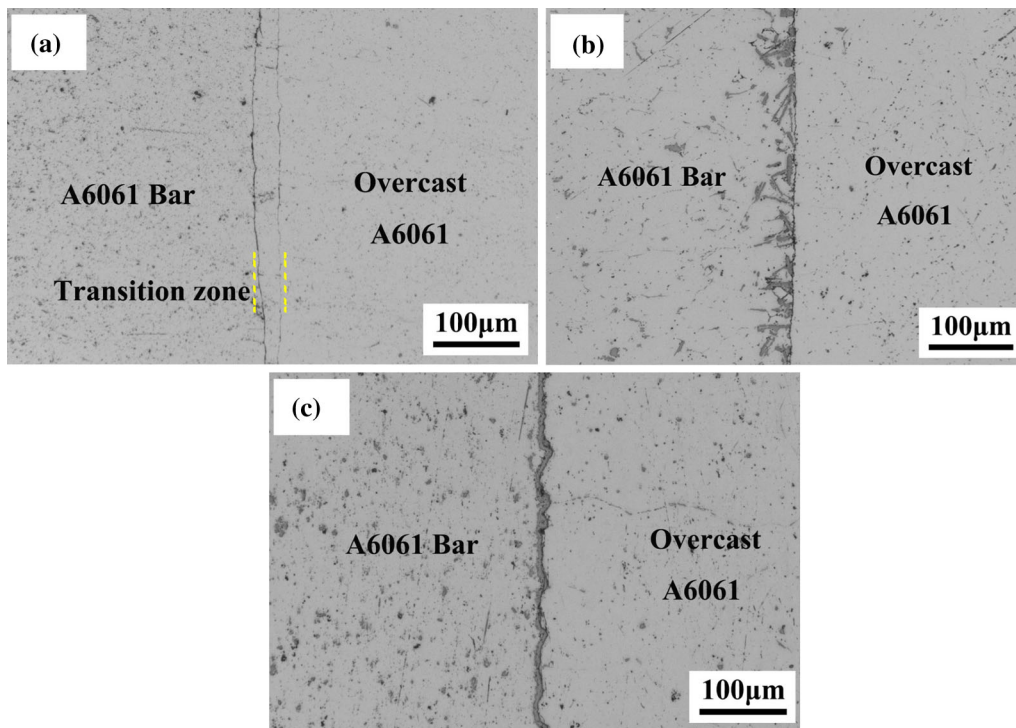

Fig. 5—Optical microstructure of the overcast joints with different thicknesses of Ni layer by gravity casting: (a) 1 μm, (b) 3 μm, and (c) 5 μm.
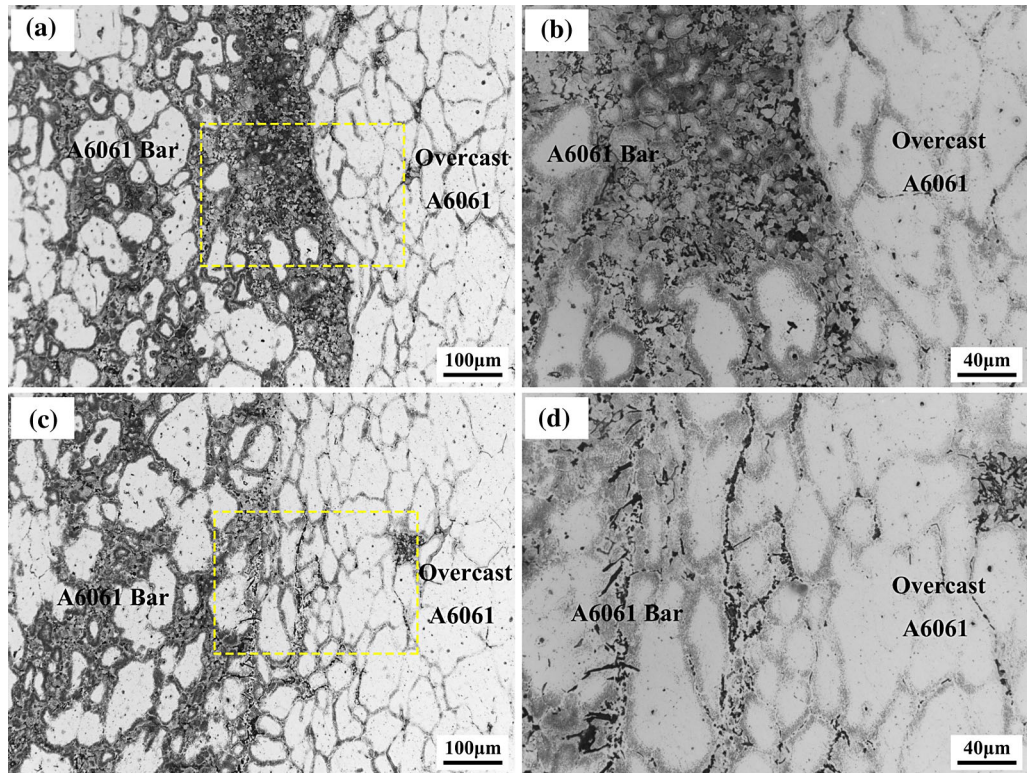
Fig. 6—Optical microstructure of the overcast joints with 3 μm Ni layer by squeeze casting: (*a, c*) 200×, (*b, d*) 500×.
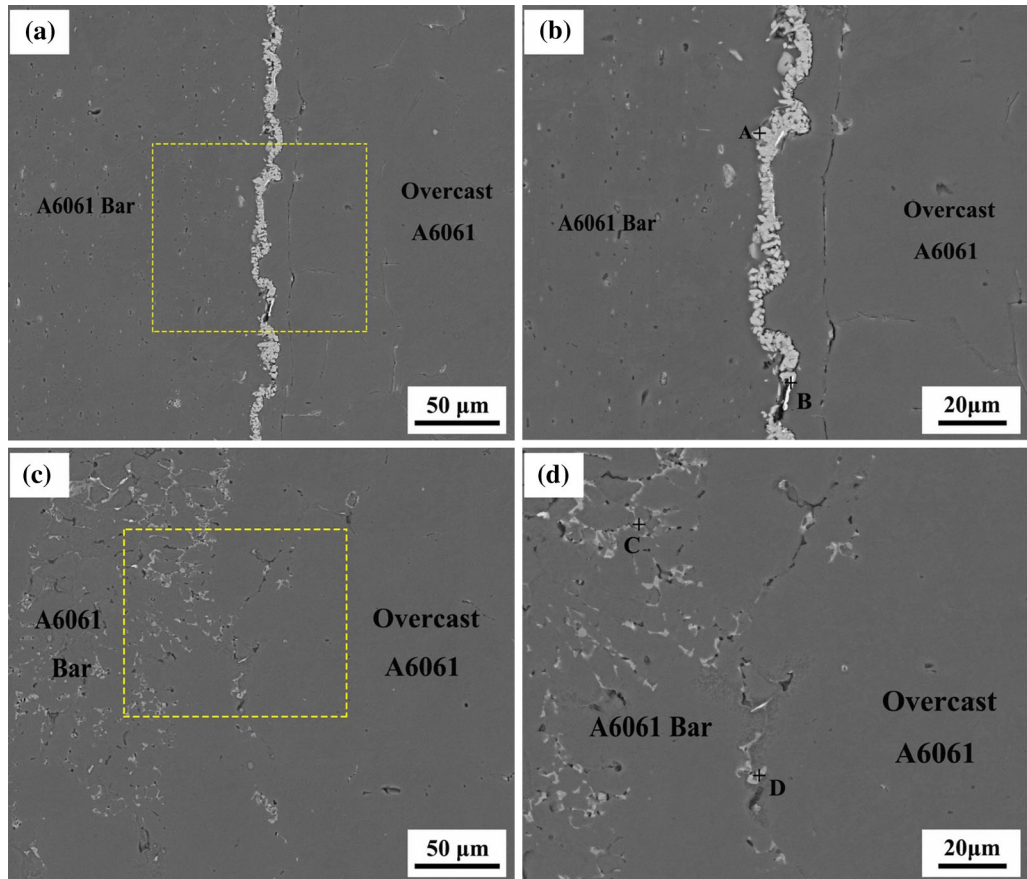

Fig. 7—SEM micrographs of the overcast joints with 3 μm Ni layer made by gravity casting (*a, b*) and squeeze casting (*c, d*).

interfacial zone. Many microcracks are detected in the cracked Al_3Ni intermetallic, which degrades the mechanical properties of the joints. Furthermore, the composition of point B demonstrates that little residual Ni particles also exist in the interfacial zone. In squeeze overcast joint, however, no coarse intermetallic and microcracks are detected. Strengthening phases distribute on both sides of the interfacial region, and their sizes dramatically decrease, which is beneficial to the mechanical properties of the joints. The composition of point C and point D confirms that these fine and dispersed phases are Ni rich, which contains a small amount of Si and Fe. Comparing Figures 7(b) and (d), it is obvious that the introduction of constant pressure during solidification greatly refines the interface microstructure and results in the formation of a discontinuous transition zone with fine and dispersed Ni-rich phases.

SEM chemical element mapping of the overcast joints in the interfacial region of the samples made by gravity casting and squeeze casting with 3 μm Ni layer is shown in Figures 8(a) and (b), respectively. In gravity casting sample, obvious interface forms in the bond area. Ni was heavily present along the bondline, whereas small amounts of Si, Mg, and Fe were present throughout the interfacial zone. However, in squeeze casting coupon, the interfacial zone exhibited less difference in Mg concentration across the bondline and essentially uniform Ni concentration. On the other hand, Si and Fe had a stronger tendency to segregate in the interfacial zone and form fine and dispersed strengthening phases, which are less likely to lower joint strength. This result is consistent with the EDS results of point C and point D, indicating that Si and Fe heavily react with Ni and form fine and dispersed Ni-rich strengthening phases.

Table I. EDS Results of the Corresponding Points in Figure 7

	Element (At. Pct)			
No.	Al	Ni	Si	Fe
A	73.5	26.5	—	—
B	16.8	83.2	—	—
C	72.7	14.0	12.7	0.6
D	80.4	13.1	6.0	0.5

C. Interfacial Mechanical Properties

Figure 9 shows the microhardness evolution across the interfacial zone of the overcast joints with varied Ni
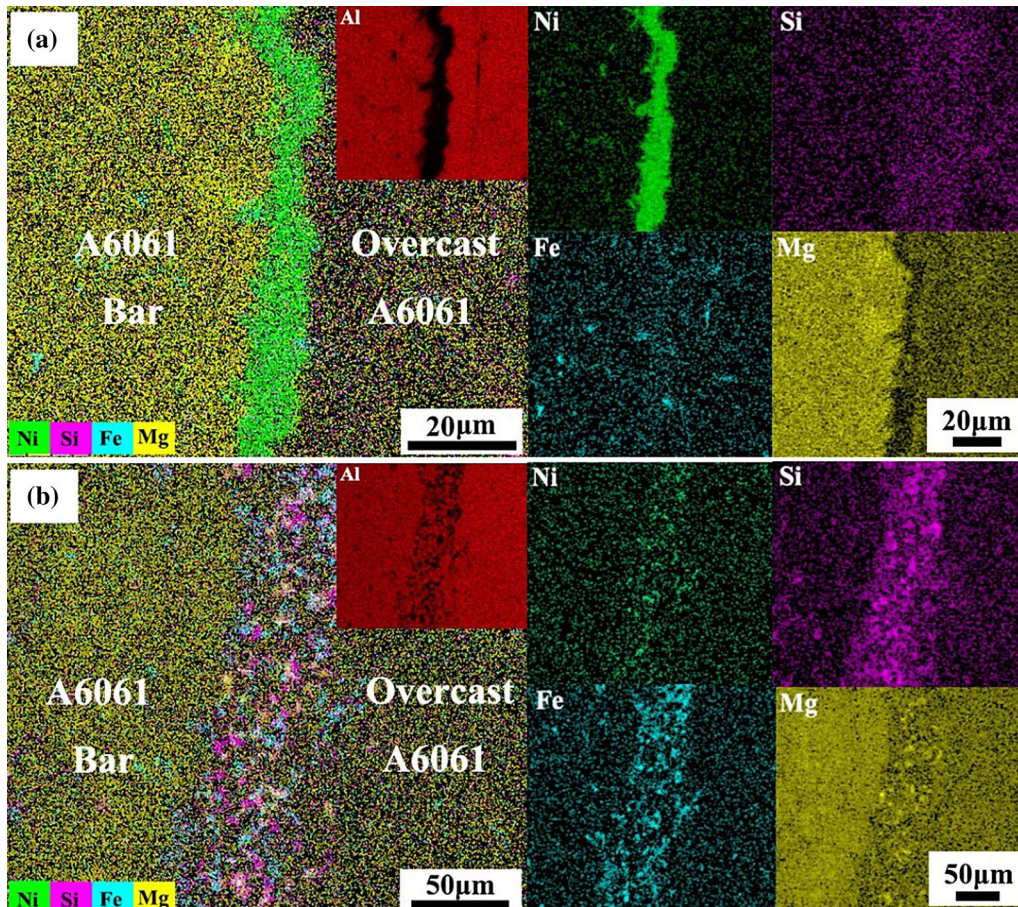

Fig. 8—SEM chemical element mapping across the interfacial region and the element mapping for the overcast joints with the Ni layer of 3 μm made by gravity casting (a) and squeeze casting (b).
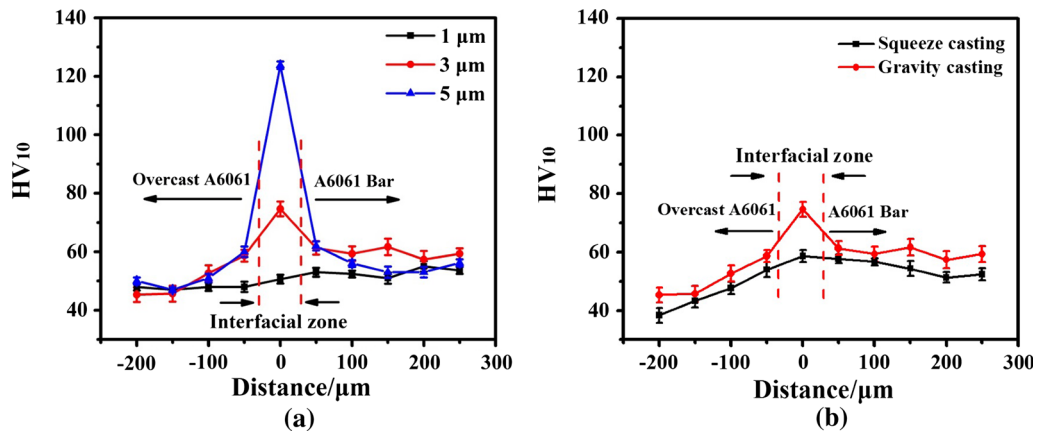
Fig. 9—Microhardness evolution across the interfacial zone of the overcast joints: (*a*) varied Ni layer thicknesses by gravity casting, (*b*) 3-μm-thick Ni layer by gravity casting and squeeze casting.

layer thicknesses by gravity casting (a) and 3 μm Ni layer by gravity casting and squeeze casting (b). In gravity casting samples, the microhardness value in the interfacial region dramatically increases with the increase of Ni layer from 1 to 5 μm. The interfacial zone with 5 μm Ni layer has a peak hardness value of 123.8 ± 1.3 HV, which is much higher than that of 1 μm and 3 μm Ni layer. Compared with 74.7 ± 2.3 HV for 3-μm-thick Ni layer, the interfacial microhardness for 1 μm Ni layer is only 50.6 ± 1.5 HV, and no obvious increment is observed across the interfacial zone. This result is consistent with the microstructure observed in the overcast joints of Figure 5 and confirms that the maximum Ni layer thickness is limited to 5 μm. In squeeze casting, with the optimal Ni layer thickness of 3 μm, the microhardness gradually increases from 38.3 ± 1.8 HV of the cast A6061 to 58.7 ± 2.1 HV of the interfacial region. Subsequently, the hardness slowly decreases to 52.0 ± 2.3 HV of the A6061 bar. Although the interfacial microhardness of 58.7 ± 2.1 HV in squeeze casting is lower than 74.7 ± 2.3 HV in gravity casting, smooth transition of the hardness value from the interfacial region to the A6061 bar indicates that the Ni-rich strengthening phases distribute uniformly along this direction in squeeze casting.

Typical tensile curves of the A6061 base material and the overcast joints made by 3-μm-thick Ni layer by gravity casting and squeeze casting are displayed in Figures 10(a) and (b). In gravity casting, the effect of the distances from bottom of the casting is obvious. In Figures 10(a) and (c), the bottom of the Al bar has a lower adhesive strength, and the bonding strength of specimens #1 and #2 is 0 MPa. With the increased distance from the bottom of the casting (specimens #3 to 5), the bonding strength gradually increases. Subsequently, the bonding strength dramatically increases for specimens #6 to #8. Compared with the A6061 base material strength of 130 MPa for sample #10, sample #7 has a maximum bonding strength of 152 MPa. However, in squeeze casting, the effect of the distances of sample locations is not obvious. Even if in the lowest position of the samples the bonding strength of the overcast joints reaches 80 MPa, with the increased

distance the bond strength gradually exceeds the base material strength (100 MPa) matrix and attains a maximum strength of 118 MPa with sample #8.

Although the achieved maximum bond strength of the overcast joints by gravity casting is higher than that by squeeze casting, the elongation of the overcast joints by gravity casting is much lower. Therefore, the tensile toughness is also introduced to further evaluate the mechanical properties of the overcast joints. Tensile toughness is calculated by using area underneath the stress-strain (σ–ε) curve. Figures 10(c) and (d) show the evolution of the tensile strength and the tensile toughness of the overcast joints with different distances from the bottom of the casting. It is apparent that the tensile toughness of the overcast joints made by squeeze casting is higher than that made by gravity casting, except for sample #8. The highest tensile toughness of samples by gravity casting and squeeze casting is 20.3 MJ/m^3 and 17.5 MJ/m^3, respectively. As discussed in previous section, fine and dispersed Ni-containing phase seems to increase the toughness of the joints while coarse and cracked Al$_3$Ni phase degrades the mechanical properties. More importantly, a constant pressure promotes the formation of fine and dispersed phases and eliminates the defects during solidification. Therefore, the overall tensile toughness of the overcast joints by squeeze casting is relatively higher than that by gravity casting.

D. Fracture Surface of the Joints

Figure 11 shows the fracture surfaces of tensile-fractured specimens made with the Ni layer of 3 μm at 993 K (720 °C) by gravity casting (a, b) and squeeze casting (c, d, e). In gravity casting, the occurrence of the cleavage plane, tear ridge, and dimples indicates the mixed fracture mode of brittle and ductile fracture. While in squeeze casting, more continuous tear ridge and dimples are observed indicating that ductile fracture mechanism is dominated for the overcast joints. Large amounts of fine and dispersed intermetallic compounds are observed at the bottom of the dimples and they play an important role in enhancing the tensile toughness of
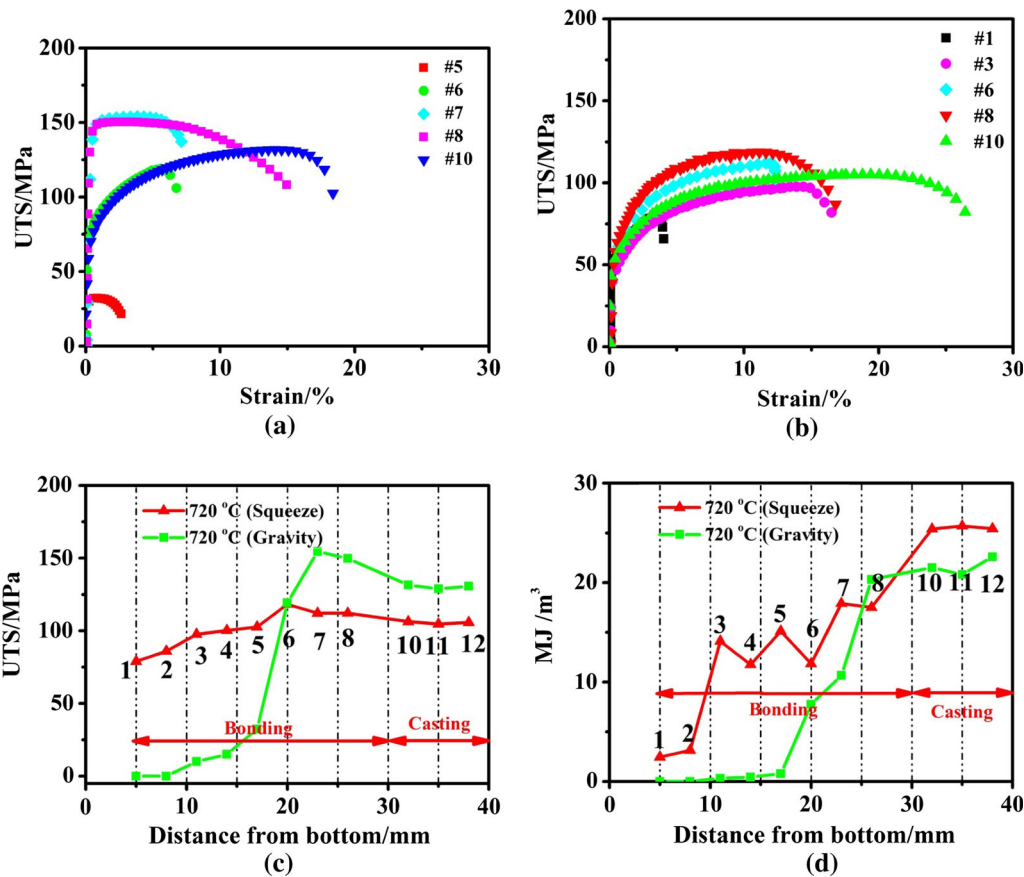
Fig. 10—Tensile curves of the overcast joints with 3-μm-thick Ni layer by gravity casting (*a*), squeeze casting (*b*), and the bonding strength (*c*) and the tensile toughness (*d*) of the joints with different distances from the bottom of the casting.

the overcast joints. Figure 11(f) shows the XRD analysis results of the overcast joints with 3 μm Ni layer by gravity casting and squeeze casting. The existence of Al, Ni, and Al$_3$Ni phase is identified in the gravity casting samples, which means that most Ni layer heavily reacts with the liquid A6061 and transforms to Al$_3$Ni phase. Compared with coarse and cracked Al$_3$Ni phase in the gravity cast samples (Figures 7(a) and (b)), fine and dispersed Ni-rich phase in the squeeze cast samples leads to the ductile fracture of the joints. Since the fracture surface may not fully propagate along the coating layer interface, the Al$_3$Ni phase was not detected by XRD.

Figure 12 exhibits the optical micrographs of the longitudinal section of the tensile-fractured specimens (#6) by gravity casting (a, b) and squeeze casting (c, d). As shown in Figures 12(a) and (b), the fracture of the overcast joints occurs at the interfacial zone with a distinct interface, indicating a poorly metallurgical bonding of the overcast joints. Combining with the XRD results in Figure 11(f), the continuous Al$_3$Ni phase in the interfacial region is confirmed. However, obvious reaction diffusion zone is detected in the squeeze cast sample. As shown in Figure 12(c), the rupture occurs in the A6061 casting materials indicating that the bond strength of the overcast joint is higher than the A6061 base material. In Figure 12(d), large amounts of fine and dispersed intermetallic phases are observed in the A6061 bar side, which indicates a higher

tendency of Ni diffusion into the Al bar under a constant pressure. There are also some intermetallic particles observed in the A6061 casting side indicating that Ni element also diffuses into the A6061 liquid during casting.

IV. DISCUSSION

A. *Choice of Ni Coating*

As shown in Figure 3, compared to the Ni coating with a thickness of 10 μm, obvious reaction diffusion zone occurs with the Cu coating of 40 μm. The diffusion distance of the Ni and Cu in the reaction zone is around 3 to 5 μm and 130 to 150 μm, respectively. The diffusion distance of the intermetallic compound can be estimated by the Fick's Law:

$$\frac{C_s - C_x}{C_s - C_0} = \mathrm{erf}\left(\frac{x}{2\sqrt{Dt}}\right), \quad [1]$$

where $C_s (= 1)$ is the Ni and Cu content in the coating, C_0 is the Ni and Cu content in the A6061 bar, which is close to 0, C_x is the Ni and Cu content at the interface. According to the EDS results of Al$_3$Ni and Al$_2$Cu, the values of C_x of Ni and Cu are 0.46 and 0.52 in weight percentage, respectively. D and t are the diffusion coefficient and diffusion time of Ni and Cu in
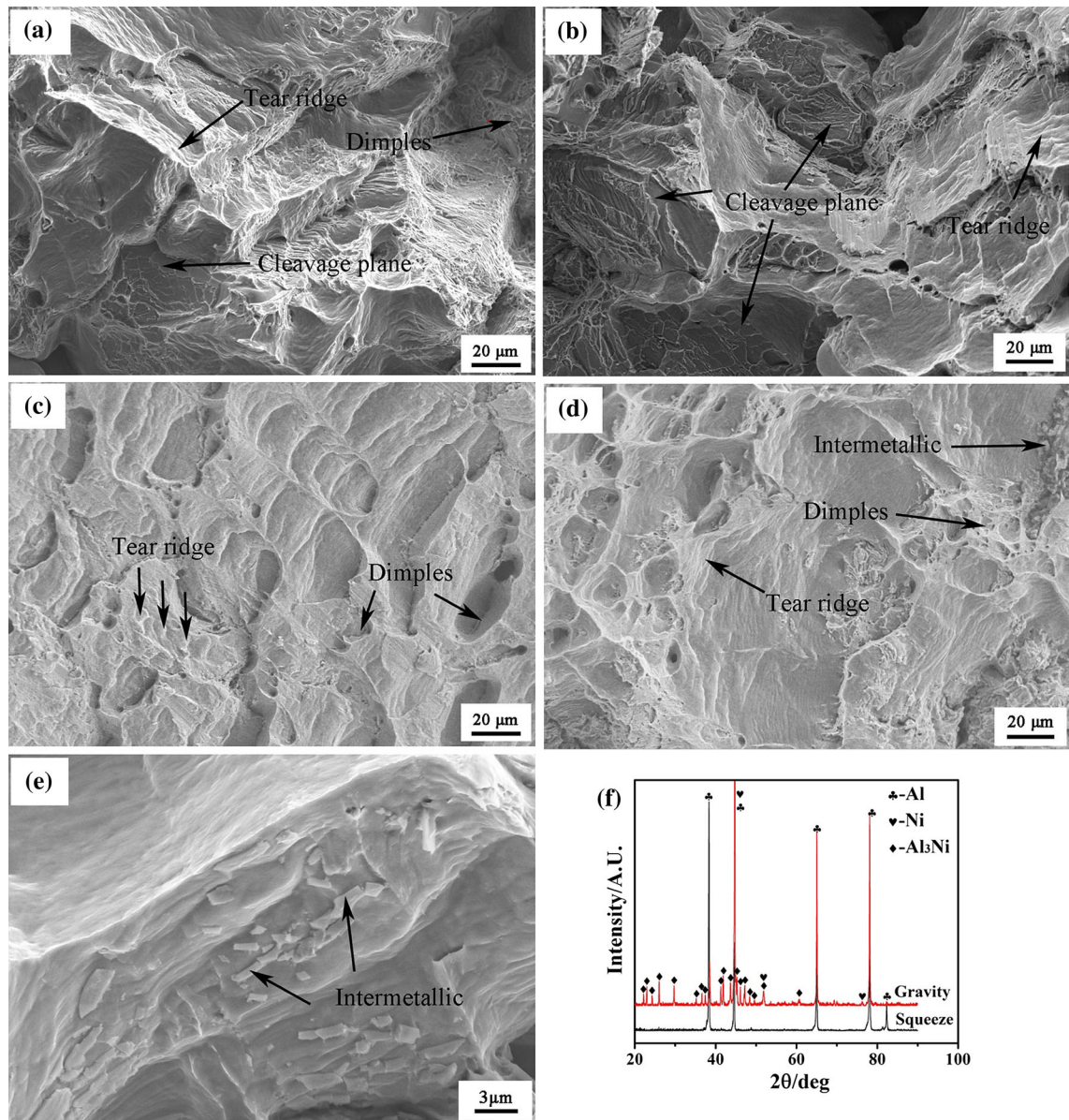
Fig. 11—Fracture surfaces of the tensile-fractured specimen #6 fabricated with 3 μm Ni layer by gravity casting (*a, b*), squeeze casting (*c, d, e*), and XRD results of the fracture surface (*f*).

casting, respectively, and *x* is the diffusion distance. The casting process is the same as that described in Reference 32 and the cooling rate of liquid Al in gravity casting is about 5 K/s, and the diffusion time is about 60 seconds. *D* at casting temperature is calculated by the Arrhenius equation:

$$D = D_0 \exp\left(\frac{-Q}{RT}\right), \qquad [2]$$

where D_0 is defined as the pre-exponential factor, *Q* is the activation energy, *R* is the gas constant, and *T* denotes the absolute temperature. The D_0 and *Q* used in this work are 4.4×10^{-4} m^2/s, 145.8 kJ/mol for Ni, and 2.0×10^{-4} m^2/s, 142.3 kJ/mol for Cu. More details about the experimental values of D_0 and *Q* in Al were discussed by Erdélyi[33] and Ceresara,[34] respectively.

The temperature range of the diffusion is 673 K to 923 K (400 °C to 650 °C).

The calculated results for the diffusion distance of Ni and Cu are 84.4 and 62.9 μm, respectively. This calculated diffusion distance of Cu is close to the observations in Figures 3(c) and (d). However, the measured diffusion distance of Ni is only 3 to 5 μm (Figure 3(b)), much less than the calculated value. This can be attributed to the formation of Al$_3$Ni phase, which impedes the diffusion of Ni in Al. Additionally, according to the calculations of Wei *et al.* [35] and Shi *et al.*,[36] the heat formation of Al$_3$Ni is −42.1 kJ/mol and Al$_2$Cu is −14.16 kJ/mol, which means that the Al$_3$Ni is more thermally stable than Al$_2$Cu. The formation of continuous and dense Al$_3$Ni layer of 3 to 5 μm heavily impedes the diffusion of Ni into the A6061 bar. Hence, accompanied
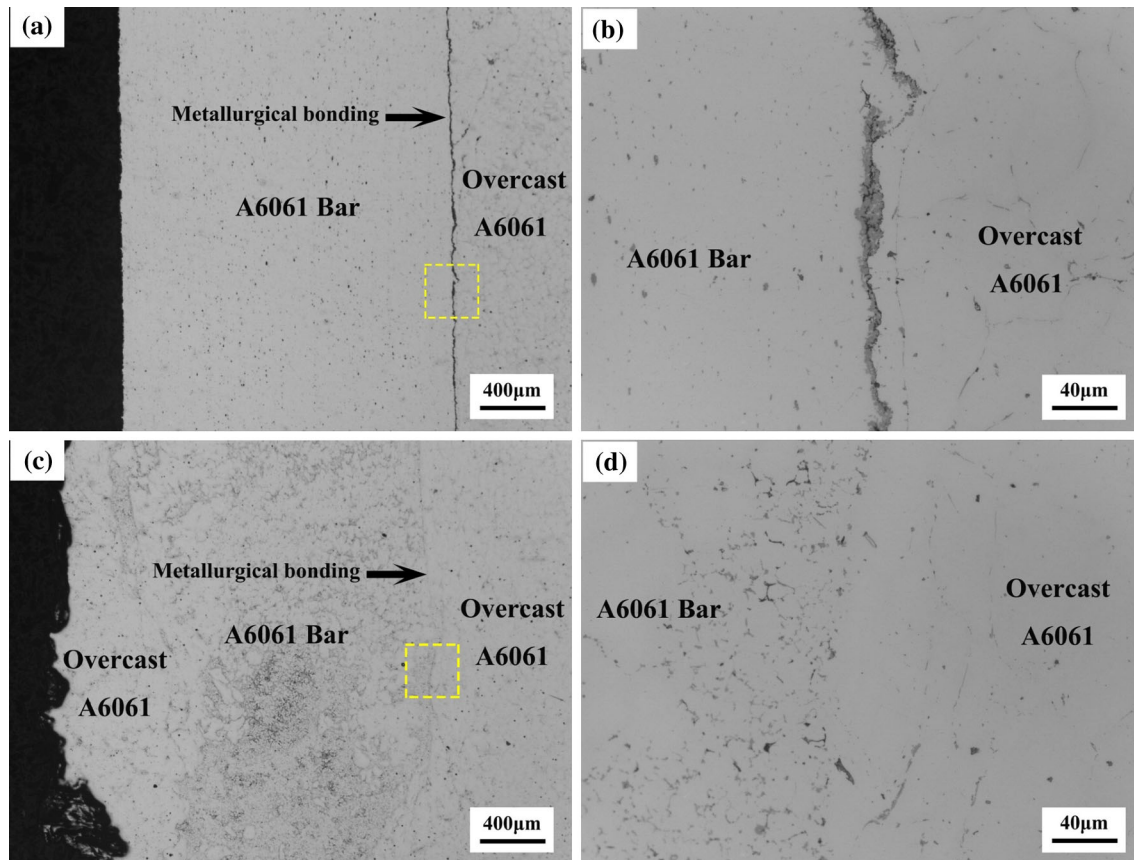
Fig. 12—Optical micrographs of a longitudinal section of the tensile-fractured specimen #6 by gravity casting (*a*, *b*) and squeeze casting (*c*, *d*).
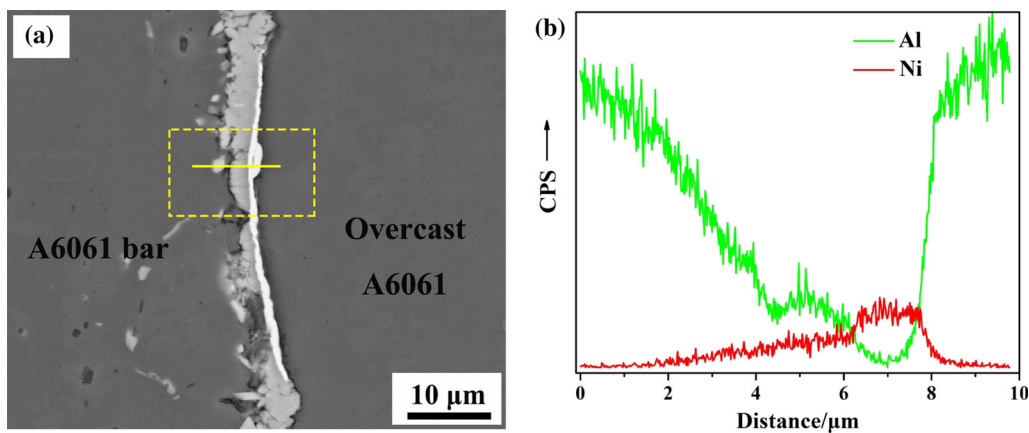

Fig. 13—The interface microstructure of the overcast joints with 5 μm Ni coating made by gravity casting (*a*) and the corresponding EDS line scan across the Ni layer (*b*).

with abundant discontinuous Al$_3$Ni phase, the overcast joints with 3 to 5 μm Ni layer is capable of protecting the A6061 bars.

B. Analysis of Interface Microstructure

To better understand the distribution of Ni element in the interfacial zone of the overcast joints, a 5-μm-thick Ni layer was introduced to highlight the evolution of the phase structure across the reaction diffusion zone during gravity casting. SEM micrograph and the EDS line scan throughout the interface are shown in Figure 13. It is clear that the Ni element segregates in the interfacial region. Owing to the lower distance from the bottom of the mold and particularly higher cooling rates of the liquid after being poured, the diffusion of Ni is rather poor, and the pure Ni particles are also detected in local area. The existence of continuous pure Ni layer implies that the 5-μm-thick Ni coating is relatively thick and the optimal thickness is limited to 3 to 5 μm.
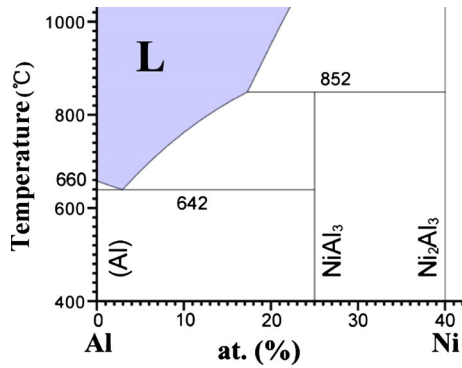
Fig. 14—The Al-Ni binary phase diagram adapted from Ref. [37].

Combining the EDS analysis across the interfacial zone in Figure 13(b) with the XRD results in Figure 11(f), and the Al-Ni binary phase diagram in Figure 14, the intermetallic compound formed in the reaction diffusion zone is identified as Al_3Ni phase. The presence of Al_3Ni intermetallic compound agrees well with the studies of Brunelli et al.[38] and Chaliampalias et al.[39] where the composition of the transition zone between Al and Ni was thoroughly investigated. The reaction layer of Al_3Ni has a width of 3 to 5 μm, further indicating that the Ni layer with a thickness of 3 to 5 μm should be sufficient for compound casting process.

While the segregation of Ni element is not observed in squeeze casting, fine and dispersed secondary phase forms in the interfacial region, indicating that the applied pressure refines the microstructure during over-casting process.[40,41] According to the Clausius–Clapeyron,

$$\frac{\Delta T_f}{\Delta P} = \frac{T_f(V_l - V_s)}{\Delta H_f}, \qquad [3]$$

where T_f is the equilibrium freezing temperature, V_l and V_s are the specific volumes of the liquid and solid, respectively, and ΔH_f is the latent heat of fusion. Substituting the appropriate thermodynamic equation for volume, the effect of pressure on freezing point may roughly be estimated as follows:

$$P = P_0 \exp\left(\frac{-\Delta H_f}{RT_f}\right), \qquad [4]$$

where P_0, R, and ΔH_f are constants. Therefore, T_f should increase with increasing pressure.[42] Compared with gravity casting, a constant pressure of 30 MPa in squeeze casting leads to the increment in equilibrium freezing temperature and promotes the interfacial reaction between molten aluminum and solid bar. Thus, the metallurgical bonding is greatly enhanced because of the formation of fine and dispersed strengthening phase.

C. *Factors Affecting the Interfacial Mechanical Properties*

The enormous difference of the mechanical properties of the overcast joints in Figure 10 indicates that the heat

transition and the applied pressure are of great importance during compound casting process. In terms of heat transition, the increased distance determines the heat transition rate. For example, in gravity casting, specimens #1 and #2 are located at the bottom of the cast ingot and possess a fast cooling rate during solidification, which inhibits the diffusion of the elements and leads to a lower bonding strength of 0 MPa. With the increasing distance away from the bottom of the cast ingot, the decreased heat transition rate promotes the diffusion of the elements and dramatically improves the bond strength of the joints. For example, the ultimate tensile strength of specimen #6 reaches 120 MPa. The effect of the applied pressure during solidification is also significant. Comparing the tensile toughness of the overcast joints made by squeeze casting and gravity casting (Figure 10(d)), under a constant applied pressure of 30 MPa, all specimens made by squeeze casting achieve a more desirable bond than those made by gravity casting except for sample #8. Because of the higher distance and lower heat transition rate, sample #8 which locates about 25 mm from the bottom possesses optimal cooling condition. Therefore, perfect bonding of overcast aluminum joints could be achieved even in gravity casting if the heat transition of the best sample seen in this work like sample #8 were accurately predicted and controlled. Based on the optimal results obtained by gravity casting, further improvement in mechanical properties of the joints by squeeze casting is expected.

V. CONCLUSIONS

In this work, bonding of aluminum alloys using Ni layer in compound casting process was studied. The influence of coating materials, coating thickness, and casting process was investigated. Based on the experimental results, the following conclusions can be withdrawn:

1. Ni coating is superior over Cu coating for the overcast joining of aluminum alloys. The reaction zone width for Ni and Cu coating is 3 to 5 μm and 130 to 150 μm, respectively. The optimal thickness of Ni coating is 3 to 5 μm.
2. In gravity casting, abundant coarse and cracked Al_3Ni phases are distributed in the interfacial zone, which are responsible for generally low mechanical properties of the overcast joints. In squeeze casting, fine and dispersed strengthening phase plays an important role in enhancing the tensile toughness of the joints.
3. In overcast joining, the heat transition and applied pressure are two key factors in determining the mechanical properties of the joints.

REFERENCES

1. C.B. Fuller, A.R. Krause, D.C. Dunand, and D.N. Seidman: *Mater. Sci. Eng. A*, 2002, vol. 338, pp. 8–16.
2. K.L. Fan, X.S. Liu, G.Q. He, and H. Chen: *Mater. Sci. Eng. A*, 2015, vol. 632, pp. 127–36.
3. M.J. Luk, F.A. Mirza, D.L. Chen, D.R. Ni, B.L. Xiao, and Z.Y. Ma: *Mater. Des.*, 2015, vol. 66, pp. 274–83.
4. L.M. Zhao and Z.D. Zhang: *Scripta Mater.*, 2008, vol. 58, pp. 283–86.
5. A. Heidarzadeh, H. Khodaverdizadeh, A. Mahmoudi, and E. Nazari: *Mater. Des.*, 2012, vol. 37, pp. 166–73.
6. P.L. Threadgill, A.J. Leonard, H.R. Shercliff, and P.J. Withers: *Int. Mater. Rev.*, 2009, vol. 54, pp. 49–93.
7. M.B. Prime, T. Gnaupel-Herold, J.A. Baumann, R.J. Lederich, D.M. Bowden, and R.J. Sebring: *Acta Mater.*, 2006, vol. 54, pp. 4013–21.
8. R. Nandan, T. Debroy, and H. Bhadeshia: *Prog. Mater. Sci.*, 2008, vol. 53, pp. 980–1023.
9. J. Hu and H.L. Tsai: *Int. J. Heat Mass. Trans.*, 2007, vol. 50, pp. 833–46.
10. P. Praveen and P.K.D.V. Yarlagadda: *J. Mater. Process. Tech.*, 2005, vol. 164, pp. 1106–12.
11. K.Y. Bae, T.H. Lee, and K.C. Ahn: *J. Mater. Process. Tech.*, 2002, vol. 120, pp. 458–65.
12. H.Y. Wang, L.M. Liu, and F. Liu: *Mater. Des.*, 2013, vol. 50, pp. 463–66.
13. X. Cao, M. Jahazi, J.P. Immarigeon, and W. Wallace: *J. Mater. Process. Tech.*, 2006, vol. 171, pp. 188–204.
14. A.K. Dubey and V. Yadava: *Int. J. Mach. Tool. Manuf.*, 2008, vol. 48, pp. 609–28.
15. E. Schubert, I. Zerner, C. Walz, and G. Sepold: *J. Mater. Process. Technol.*, 2001, vol. 115, pp. 2–8.
16. G. Xu, A.A. Luo, Y. Chen, and A.K. Sachdev: *Mater. Sci. Eng. A*, 2014, vol. 595, pp. 154–58.
17. J. Zhang, G. Luo, Y. Wang, Q. Shen, and L. Zhang: *Mater. Lett.*, 2012, vol. 83, pp. 189–91.
18. B. Mvola, P. Kah, and J. Martikainen: *Inter. J. Mech. Mater. Eng.*, 2014, vol. 9, pp. 21–32.
19. K.J.M. Papis, J.F. Loffler, and P.J. Uggowitzer: *Mater. Sci. Eng. A*, 2010, vol. 527, pp. 2274–79.
20. E. Hajjari, M. Divandari, S.H. Razavi, S.M. Emami, T. Homma, and S. Kamado: *J. Mater. Sci.*, 2011, vol. 46, pp. 6491–99.
21. P. Praveen, P.K.D.V. Yarlagadda, and M.J. Kang: *J. Mater. Process. Technol.*, 2005, vol. 164, pp. 1113–19.
22. K.J.M. Papis, B. Hallstedt, J.F. Loffler, and P.J. Uggowitzer: *Acta Mater.*, 2008, vol. 56, pp. 3036–43.
23. M. Rubner, M. Gunzl, C. Korner, and R.F. Singer: *Mater. Sci. Eng. A*, 2011, vol. 528, pp. 7024–29.
24. T. Liu, Q. Wang, Y. Sui, Q. Wang, and W. Ding: *Mater. Des.*, 2015, vol. 68, pp. 8–17.
25. S. Kundu, G. Anand, and S. Chatterjee: *Metall. Mater. Trans. A*, 2013, vol. 44A, pp. 2196–2211.
26. J. Zhang, Q. Shen, G.Q. Luo, M.J. Li, and L.M. Zhang: *Mater. Des.*, 2012, vol. 39, pp. 81–86.
27. S.Y. Shin, M.W. Ko, D.C. Cho, C.H. Lee, K.S. Shin, and K. Park: *J. Mater. Sci. Lett.*, 2002, vol. 21, pp. 903–06.
28. J. Xu, J. Tao, Z.Y. Chen, W.H. Zhu, S.Y. Jiang, and Z. Xu: *Surf. Coat. Technol.*, 2007, vol. 202, pp. 577–82.
29. S.H. Chen, J.H. Huang, K. Ma, H. Zhang, and X.K. Zhao: *Mater. Lett.*, 2012, vol. 79, pp. 296–99.
30. M. Sun, S.T. Niknejad, G. Zhang, M.K. Lee, L. Wu, and Y. Zhou: *Mater. Des.*, 2015, vol. 87, pp. 905–13.
31. T. Liu, Q. Wang, Y. Sui, Q. Wang, and W. Ding: *Mater. Des.*, 2016, vol. 89, pp. 1137–46.
32. S. Zhang, G.Y. Yuan, C. Lu, and W.J. Ding: *J. Alloy. Compd.*, 2011, vol. 509, pp. 3515–21.
33. G. Erdélyi, D.L. Beke, F.J. Kedves, and I. Gödény: *Philos. Mag. B*, 1978, vol. 38, pp. 445–62.
34. S. Ceresara: *Phys. Stat. Solid. B*, 1968, vol. 27, pp. 517–20.
35. Y. Wei, J. Li, J. Xiong, and F. Zhang: *Eng. Sci. Technol. Int. J.*, 2016, vol. 19, pp. 90–95.
36. D. Shi, B. Wen, R. Melnik, S. Yao, and T. Li: *J. Solid. State. Chem.*, 2009, vol. 182, pp. 2664–69.
37. J. Miettinen: *Calphad.*, 2005, vol. 29, pp. 40–48.
38. K. Brunelli, L. Peruzzo, and M. Dabala: *Mater. Chem. Phys.*, 2015, vol. 149, pp. 350–58.
39. D. Chaliampalias, S. Andronis, N. Pliatsikas, E. Pavlidou, D. Tsipas, and S. Skolianos: *Surf. Coat. Technol.*, 2014, vol. 255, pp. 62–68.
40. D.J. Lloyd, M. Gallerneault, and R.B. Wagstaff: *Metall. Mater. Trans. A*, 2010, vol. 41A, pp. 2093–2103.
41. S. Lü, S. Wu, W. Dai, C. Lin, and P. An: *J. Mater. Proces. Technol.*, 2012, vol. 212, pp. 1281–87.
42. M.R. Ghomashchi and A. Vikhrov: *J. Mater. Proces. Technol.*, 2000, vol. 101, pp. 1–9.